

Measurement and analysis of differential work hardening behavior of pure titanium sheet using spline function

Mantaro Ishiki · Toshihiko Kuwabara ·
Yasuhiro Hayashida

Received: 20 June 2010 / Accepted: 13 December 2010 / Published online: 21 January 2011
© Springer-Verlag France 2011

Abstract Biaxial stress tests and in-plane tension/compression tests of pure titanium sheet (JIS #1) have been carried out in order to elucidate its anisotropic plastic deformation behavior under linear stress paths. Contours of plastic work and the directions of plastic strain rates at different levels of plastic work have been precisely measured in the stress space. The measured work contours bulged significantly toward the equibiaxial direction and showed strong asymmetry, and moreover, changed its shapes significantly with increasing plastic work (differential work hardening). Using the data of the measured work contours, the applicability of selected anisotropic yield functions, i.e., Hill's quadratic, the Yld2000-2d and Cazacu's yield functions, to the accurate prediction of the plastic deformation behavior of the pure titanium has been discussed. It was found that these yield functions were not able to reproduce the measured data. A new method for analyzing the differential work hardening behavior of the pure titanium sheet has been developed. This method uses the spline function of Bezier curves which approximates a work contour, inspired by the methodology proposed by Vegter and Boogaard (Int. J. Plasticity 22 (2006) 557-580). The procedure for determining the spline function is described in detail. The calculated results have been in good agreement with the differential work hardening behavior of the pure titanium sheet.

Keywords Pure titanium sheet · Yield function · Differential work hardening · Anisotropy · Biaxial stress

Introduction

Pure titanium has high corrosion resistance and therefore has mainly been applied to industrial chemical equipment and heat exchangers. The demand for them has increased lately in recent years. However, since pure titanium has a low Young's modulus and strong in-plane anisotropy, it does not lend itself well to press forming. In order to achieve time and cost effectiveness in the press forming of pure titanium sheet, it is vital to accurately predict potential defects in the resulting parts using finite element simulations and to determine optimum forming conditions. To do this, it is critical that an accurate constitutive model for pure titanium sheet be established [1].

The authors investigate the work hardening behavior of pure titanium sheet under many linear stress paths and measured the plastic work contours in the first, second and fourth quadrants of a principal stress space [2]. We found that: (a) the pure titanium showed strong in-plane anisotropy with respect to flow stresses and r -values; (b) the plastic work contours show significant asymmetry between the upper and lower sides of the line $\sigma_x = \sigma_y$, and (c) the material exhibited significant differential work hardening [2]; the degree of asymmetry of successive work contours decreases with increasing plastic work. Moreover, we found that the conventional anisotropic yield functions are not able to perfectly reproduce the deformation behavior of the pure titanium under biaxial loading.

Vegter and Van den Boogaard [3] proposed a yield function which is capable of constructing a smooth yield locus in the principal stress space using a set of quadratic

M. Ishiki (✉) · T. Kuwabara
Tokyo University of Agriculture and Technology,
2-24-16, Nakamachi,
Koganei, Tokyo 184-8588, Japan
e-mail: ishiki-mantaro@nite.go.jp

Y. Hayashida
Kobe Steel, Ltd.,
5-5, Takatsukadai 1-chome,
Nishi-ku, Kobe, Hyogo, Japan

Bezier interpolations between pre-determined stress states: equibiaxial, plane strain, uniaxial and pure shear. One of the merits using Bezier interpolations is the flexible representation of a yield locus by direct use of biaxial stress test results as reference points.

In this study, we utilize Vegter's idea of constructing a yield locus piece by piece to determine the approximation curves reproducing the observed plastic work contours of the pure titanium above mentioned. The analysis method proposed in this study is, however, different from Vegter's method. Vegter's method does not ensure the smooth variation of the directions of plastic strain rates with loading directions. On the other hand, our method utilizes Bezier curves also to interpolate the relation between the directions of plastic strain rates and loading directions. Accordingly, the method ensures the smooth variation of the directions of plastic strain rates with loading directions, as well as the shapes of successive plastic work contours. This method is capable of analyzing the differential work hardening behavior of the pure titanium, i.e., the continuous change in the shapes of the work contours and in the directions of plastic strain rates without depending on a specific yield function. This method is also useful for checking whether the differential work hardening behavior of the pure titanium follows the normality flow rule.

Material testing methods for measuring the plastic deformation behavior of pure titanium sheet

In this chapter, the material testing methods for measuring the plastic deformation behavior of pure titanium sheet are described. The x - and y -axes are defined as being along the rolling and transverse directions of the material, respectively.

Test material

The test material used in this study was 0.5 mm thick commercial pure titanium sheet (JIS #1). The chemical composition and the mechanical properties of the material are shown in Tables 1 and 2, respectively. The mechanical properties were measured using uniaxial tensile tests at 0, 22.5, 45, 67.5 and 90° directions with respect to the rolling direction. The material had strong in-plane anisotropy: $\sigma_{0.2}$ was 25% larger at 90° than at 0° and the r -value was three times larger at 90° than at 0°. Such large anisotropy of pure titanium sheet were also reported in [4].

Table 1 Chemical composition of the pure titanium sheet (%)

H	O	N	Fe	C	Ti
0.013	0.15	0.03	0.20	0.08	Bal.

Table 2 Mechanical properties of the pure titanium sheet (JIS #1)

Cutting direction	E /GPa	$\sigma_{0.2}^{*1}$ /MPa	n^{*1}	n^{*2}	r -value ^{*3}
0°	96	178	0.14	0.55	1.7
22.5°	99	192	0.13	0.79	1.9
45°	96	206	0.13	1.04	3.7
67.5°	98	224	0.12	0.044	4.2
90°	104	225	0.10	0.13	5.0

*1 Approximated using $\sigma = c(\varepsilon_0 + \varepsilon^p)^n$ for $\varepsilon^p = 0.002$ – 0.04

*2 Approximated using $\sigma = c(\varepsilon_0 + \varepsilon^p)^n$ for $\varepsilon^p \geq 0.05$

*3 Average value for $\varepsilon^p = 0.03$ to 0.20 measured from the change in width and length of the specimen gauge section

Figure 1 shows the (0001) pole figure of the test material observed using EBSP (Electron Backscatter Diffraction Pattern). The preferred orientation of (0001) pole is symmetrically-tilted around the axis of rolling direction (RD) toward the transverse direction. The average grain size was approximately 35 μm .

Testing methods

Biaxial tensile test

Figure 2 shows the geometry of the cruciform specimen used in biaxial tensile tests. It is identical to that used by Kuwabara et al. [5]. Biaxial tensile forces (F_x , F_y) were applied to the specimen and the normal strain components (ε_x , ε_y) were measured using strain gauges mounted at the center of the gauge section. The true stress components (σ_x , σ_y) in the gauge section were determined by dividing the measured forces (F_x , F_y) by the current cross-sectional area which, in turn, was determined from the measured values of plastic strain components (ε_x^p , ε_y^p) using the assumption of constant volume. For more details of the testing apparatus, refer to [5].

In the biaxial tensile tests on materials with low n -values, like the pure titanium used in this study, fracture occurs at an early stage of plastic deformation in one of the arms of the cruciform specimen. In an effort to observe the plastic deformation behavior over a much larger range of plastic strain, combined tension-internal pressure tests were carried out using tubular specimens. These were made using the same single lot of the pure titanium sheet used to make the cruciform specimens. Many linear stress paths consisting of the axial and circumferential stress components (σ_ϕ , σ_θ) were applied to the tubular specimens using the closed-loop electrically servo-controlled tension-internal pressure testing apparatus developed in [6]. For more details, refer to [6] and [7].

The tubular specimens were manually bent and welded. Hereafter, the axial and circumferential directions of the

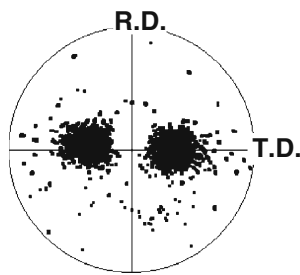


Fig. 1 (0001) pole figure of the pure titanium sheet (JIS #1)

tube are denoted ϕ and θ , respectively. In preliminary experiments, the fracture strength of the weld was found to be much lower than that of the parent material. With $\sigma_\theta > \sigma_\phi$, fracture occurred at the weld before sufficiently large plastic deformation could be applied to the parent material. Therefore, it was decided to make two types of tubular specimens, Types A and B, as shown in Fig. 3. In Type A, the rolling direction of the original sheet is parallel to the axial direction of the tubular specimen, whereas in Type B, it is parallel to the circumferential direction. Biaxial tensile tests were performed so as to make the maximum stress direction parallel to the axial direction. To avoid changes to the mechanical properties of the test material, thermal stress relief was not applied to the tubular specimens.

The axial and circumferential strains in the tubular specimens were measured using strain gauges (Tokyo Sokki Kenkyujo Co., YFLA-2) mounted at the center of the specimen. Stress components (σ_ϕ , σ_θ) were determined using the equilibrium equations for the axial and radial directions [7].

Combined tension-compression test

In order to observe the biaxial deformation behavior of the pure titanium in the second and fourth quadrants of

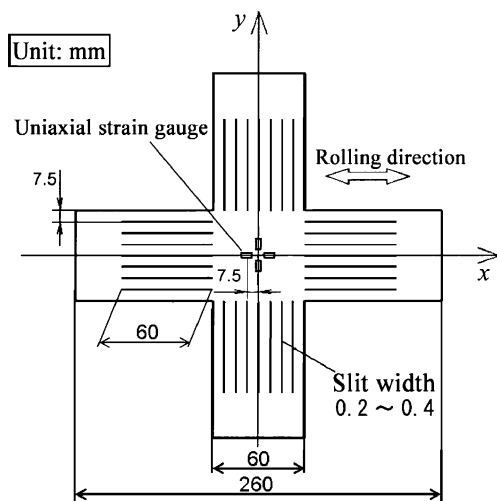


Fig. 2 Cruciform specimen for biaxial tensile test

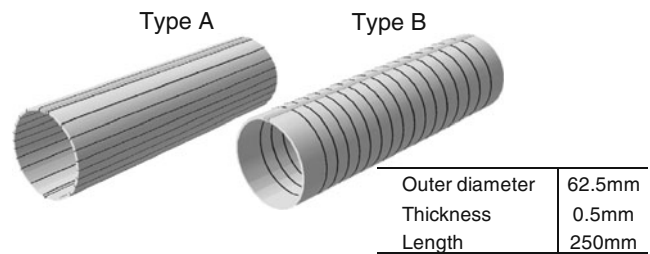


Fig. 3 Two types of tubular specimens used in biaxial tensile tests. The thin lines indicate the rolling direction of the as-received pure titanium sheet

stress space, combined tension-compression tests were carried out using a newly designed specimen, shown in Fig. 4. Combined tensile and compressive forces were applied to the gauge section of the specimen in the longitudinal and transverse directions, respectively. The longitudinal and transverse strains were measured using a biaxial strain gauge (Tokyo Sokki Kenkyujo Co., FCA 1-11) mounted at the center of the gauge section. The same testing machine as that used in the biaxial tension tests was used for the combined tension-compression tests with special jigs installed to allow combined tension-compression forces to be applied to the specimen. For more details, refer to [8].

Uniaxial in-plane compression test

Hexagonal close packed metals generally exhibit a strength differential (SD) between tension and compression [4, 9]. In order to check whether the pure titanium used in this study also exhibits such a SD, uniaxial in-plane compression tests were carried out using the uniaxial specimen shown in Fig. 5 and the in-plane tension-compression testing apparatus shown in Fig. 6. The methodology for applying a in-plane compression force to a sheet specimen was first developed in [10] and further elaborated into a continuous stress reversal test in [11]. The testing apparatus consists of a pair of comb-shaped dies which sandwich a sheet specimen with blank-holding pressure applied. This allows continuous tension-compression stress-

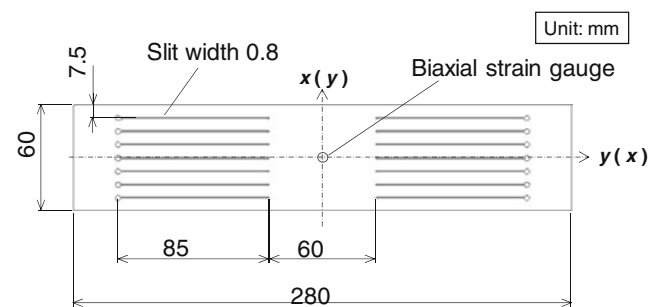


Fig. 4 Specimen for combined tension-compression test

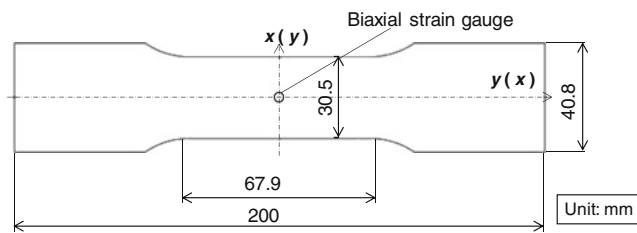


Fig. 5 Specimen for in-plane uniaxial compression test

strain curves to be obtained without buckling. For more details, refer to [11].

Test procedure

All tests mentioned above were carried out under linear stress paths with a constant von Mises equivalent stress rate of 0.5 MPa/s. Measured values of load and strain were recorded at an interval of 0.5 s.

The stress ratios applied to the test material were $\sigma_x:\sigma_y=1:0, 4:1, 2:1, 4:3, 1:1, 3:4, 1:2, 1:4$, and 0:1 in the first quadrant of stress space and 0:-1, -1:2, -1:1, -2:1, -1:0, 1:-2, 1:-1 and 2:-1 in the second and fourth quadrants of stress space. The difference between reference and measured stress values was less than ± 0.5 MPa in any loading paths.

In order to quantitatively evaluate the yielding and the subsequent work hardening characteristics of the pure titanium sheet under combined stress states, the evolution of contours of plastic work in the principal stress space were measured [2]. The stress-strain curve obtained from the uniaxial tensile test in the rolling direction was chosen as a reference data for work hardening. First, the uniaxial true stresses σ_0 and the plastic work W per unit volume corresponding to particular values of offset logarithmic plastic strains ε_0^p were determined. Then, the uniaxial true stress σ_{90} obtained from a uniaxial tensile test in the transverse direction of the material and the biaxial true stress components $(\sigma_x:\sigma_y)$, at which the same amount of plastic work as W was consumed, were determined and

plotted in the principal stress space. These stress points define a contour of plastic work corresponding to a particular value of ε_0^p . When ε_0^p is taken to be sufficiently small, the corresponding work contour can be practically viewed as an initial yield locus.

In order to verify whether the measured work contours can be viewed as plastic potential, the direction of plastic strain rate, β , were also measured using the equation $\beta = \tan^{-1}(d\varepsilon_y^p/d\varepsilon_x^p)$ at every stress point, where $d\varepsilon_x^p$ and $d\varepsilon_y^p$ are the plastic strain increments in the rolling and transverse directions, respectively, measured using strain gauges at an interval of approximately 10 seconds.

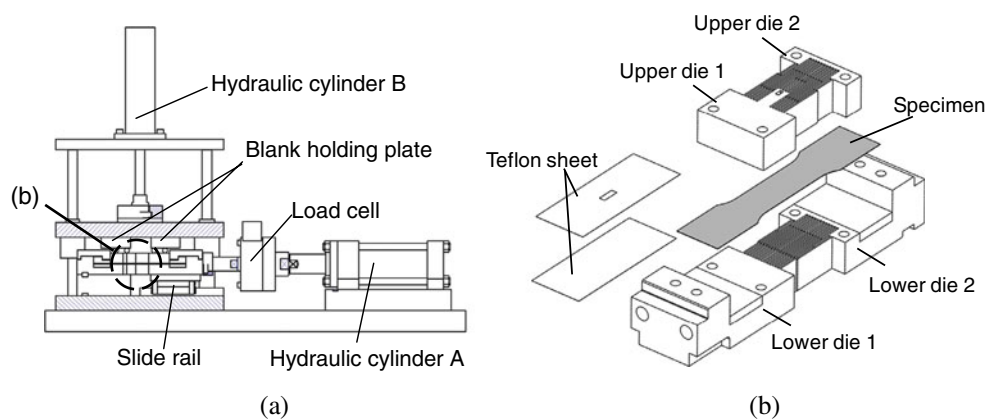
Two or three specimens were tested for each linear loading experiment. The repeatability of stress measurement between each test was less than ± 1 MPa. The measurement error of stress value was estimated to be less than ± 0.5 MPa. The measurement error of β was estimated to be less than $\pm 2.5^\circ$.

Experimental results

Differential work hardening behavior in the first quadrant of stress space

Figure 7 shows the stress points defining contours of plastic work for different levels of ε_0^p in the first quadrant of stress space. The stress components of the stress points comprising a contour of plastic work are normalized by σ_0 corresponding to the ε_0^p . The work contours for $\varepsilon_0^p = 0.001$ and 0.002 were determined using cruciform specimens. The work contours for $\varepsilon_0^p = 0.002$ were determined using tubular specimens. The adhesion limit of the strain gauges limited the measurable maximum plastic strain to $\varepsilon_0^p = 0.085$. The normalized work contour for $\varepsilon_0^p = 0.001$, which can be practically regarded as an initial yield locus, bulges significantly in the range of $\sigma_x:\sigma_y=0:1$ to 4:3 and shows strong asymmetry with respect to the line $\sigma_x=\sigma_y$. The degree of asymmetry of the initial yield locus is more

Fig. 6 Experimental apparatus for applying in-plane tension-compression stress reversals to a sheet specimen. **a** Comb-shaped dies. **b** Testing apparatus



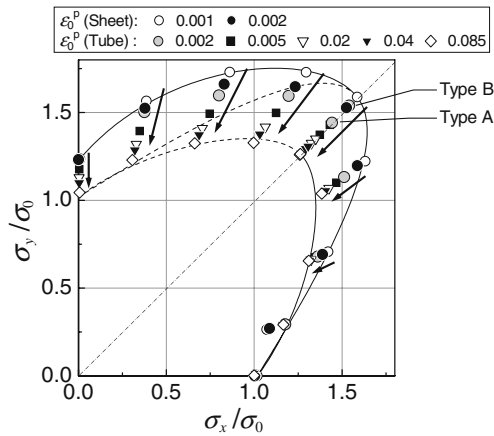


Fig. 7 Contours of plastic work for the pure titanium sheet in the first quadrant of stress space

significant in pure titanium sheet than in steel alloys [5, 6, 12] and an aluminum alloy [7].

There is a discrepancy between the work contours for $\epsilon_0^p = 0.002$ determined using cruciform specimens and tubular specimens. It is attributed to the prestrain applied to the tubular specimens during the fabrication process. The amount of total strain applied to the tubular specimens during bending is estimated to be $t/D \approx 0.008$, where t is the sheet thickness and D is the tube diameter. Therefore, the plastic prestrain applied to the tubular specimens was approximately 0.006.

It is clearly observed that the degree of bulging and asymmetry of the successive work contours decreases with increasing ϵ_0^p . This work hardening behavior of the pure titanium sheet exemplifies the terminology “*differential work hardening*” suggested in [2].

In order to quantitatively analyze the differential work hardening behavior of the test material, the shape ratios of stress points comprising a work contour were determined for each stress ratio. The shape ratio is defined as L/L_0 , where L is the distance between a stress point and the origin in the non-dimensional stress space, and L_0 is the value of L at $\epsilon_0^p = 0.085$. The variation of the shape ratio L/L_0 for each loading direction with ϵ_0^p is shown in Fig. 8. L/L_0 steeply decreased immediately after the commencement of plastic deformation and the rate of decrease appears to gradually converge to a constant value. The maximum rate of decrease of L/L_0 was observed for $\sigma_x:\sigma_y=0:1$.

Figure 9 shows the variation of the directions of plastic strain rates at every stress ratio with ϵ_0^p . The horizontal axis of the graph represents the stress ratio in terms of the direction angle φ of stress vector in stress space. At the commencement of plastic deformation, $\epsilon_0^p = 0.002$, the stress ratio that gave the plane strain tension in the rolling direction ($\beta=0^\circ$) was approximately $\varphi=41.2^\circ$ ($\sigma_x:\sigma_y=8:7$). The value is much closer to the equibiaxial direction ($\varphi=$

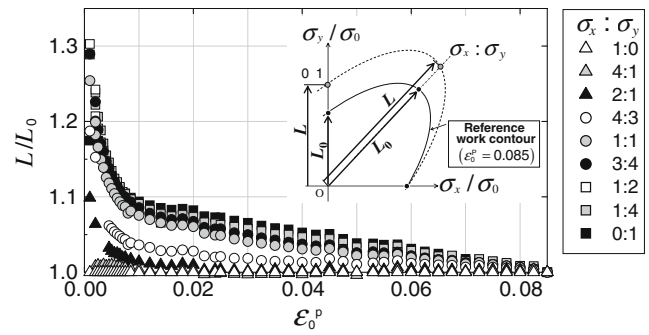


Fig. 8 Variation of the shape ratios of stress points (L/L_0) for every loading direction with offset logarithmic plastic strain

45°) than that of an isotropic material, $\varphi=26.5^\circ$ ($\sigma_x:\sigma_y=2:1$). The β measured under equibiaxial tension ($\varphi=45^\circ$) was 22° , exhibiting strong in-plane anisotropy.

The solid line in the figure approximates the measured data at $\epsilon_0^p = 0.085$ in a range of $\varphi=0$ to 45° , and the dashed line is obtained by rotating the solid curve 180° around the point of $(\varphi, \beta)=(45^\circ, 45^\circ)$. It is clearly seen in the figure that the values of β at every stress path, φ , approach the solid and dashed lines with the increase of ϵ_0^p , as indicated by the arrows in the figure. This behavior of β accords with the general trend of the work contours shown in Fig. 7; the asymmetry with respect to the line $\sigma_x=\sigma_y$ diminishes with the increase of ϵ_0^p .

Strength differential between tension and compression

Figure 10 shows the true stress-logarithmic plastic strain curves in the rolling and transverse directions of the test material. In the rolling direction, the tensile flow stresses are approximately 30% (30 MPa) higher than the compressive ones at $\epsilon_0^p = 0.002$, exhibiting significant SD. In the transverse direction, the tensile and compressive flow stresses are nearly equal to each other in a range of

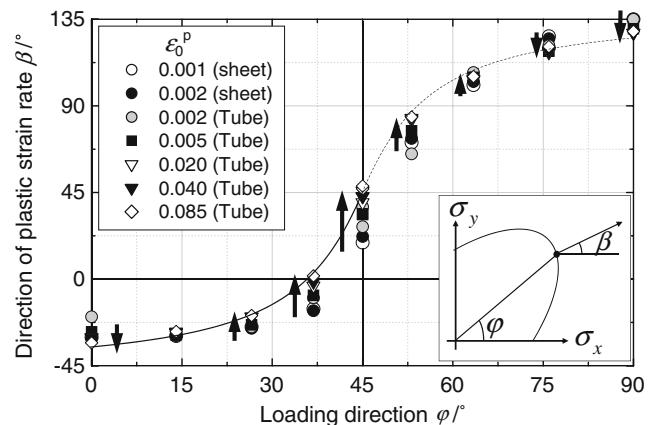


Fig. 9 Directions of plastic strain rates at different levels of offset logarithmic plastic strain ϵ_0^p

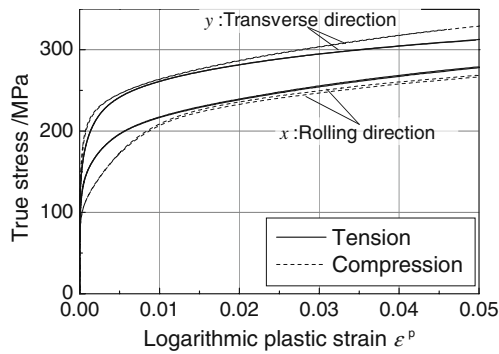


Fig. 10 Comparison of stress-strain curves for uniaxial tension and compression

$\epsilon_0^p \leq 0.02$, while the compressive flow stress gradually becomes higher than the tensile one in a range of $\epsilon_0^p > 0.02$.

Differential work hardening behavior in the second and fourth quadrants of stress space

Figure 11 shows the stress points comprising the contours of plastic work for different levels of ϵ_0^p in the second and fourth quadrants of stress space. The stress values are normalized by σ_0 corresponding to the ϵ_0^p of every contour. It was possible to perform the combined tension-compression tests up to a work hardening level of $\epsilon_0^p = 0.04$ without buckling.

The differential work hardening behavior in the second and fourth quadrants of stress space was different from that in the first quadrant shown in Fig. 7. The trend of the work contours in the second quadrant changed at $\epsilon_0^p \approx 0.01$ from bulging to receding. In contrast, the work contours in the fourth quadrant persistently receded with plastic deformation. In order to quantitatively analyze the differences of the differential work hardening behavior between both quadrants, the distance of every stress point from the origin were calculated. Figure 12 (a1) and (b1) shows the variation of L with ϵ_0^p in the second and fourth quadrants of stress space,

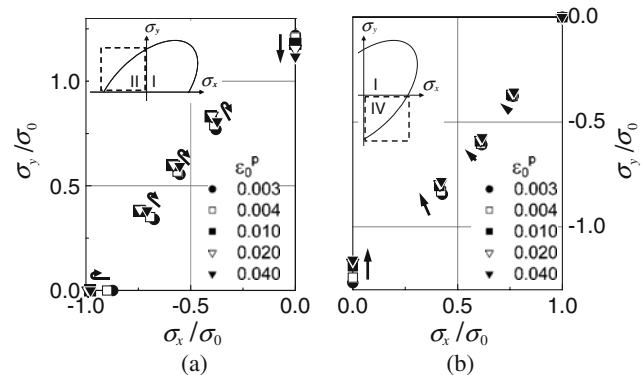


Fig. 11 Contours of plastic work in the second **a** and fourth **b** quadrants of stress space

respectively. It is clear that the L in the second quadrant increased with ϵ_0^p at the early stages of plastic deformation and began to gradually decrease at $\epsilon_0^p \approx 0.01$. Figure 12 (a2) and (b2) shows the variation of the directions of plastic strain rates β with ϵ_0^p in each quadrant. The β in the second quadrant shown in (a2) decreased with ϵ_0^p at the commencement of plastic deformation and were near constant in a range of $\epsilon_0^p \geq 0.01$. On the other hand, the β in the fourth quadrant shown in (b2) decreased monotonically with ϵ_0^p .

Analysis method

In order to explain a new methodology for determining approximation curves for measured work contours, we use the experimental data measured in the biaxial stress tests of a steel sheet [8], as shown in Fig. 13. Figure 13 (a) shows a normalized work contour in the first and second quadrants in principal stress space for $\epsilon_0^p = 0.002$. The stress components σ_x and σ_y are normalized by σ_0 , the uniaxial true stress for $\epsilon_0^p = 0.002$ in the rolling direction. Figure 13 (b) shows the relation between the direction of plastic strain rate β and the loading direction φ in stress space, corresponding to the stress points in Fig. 13 (a).

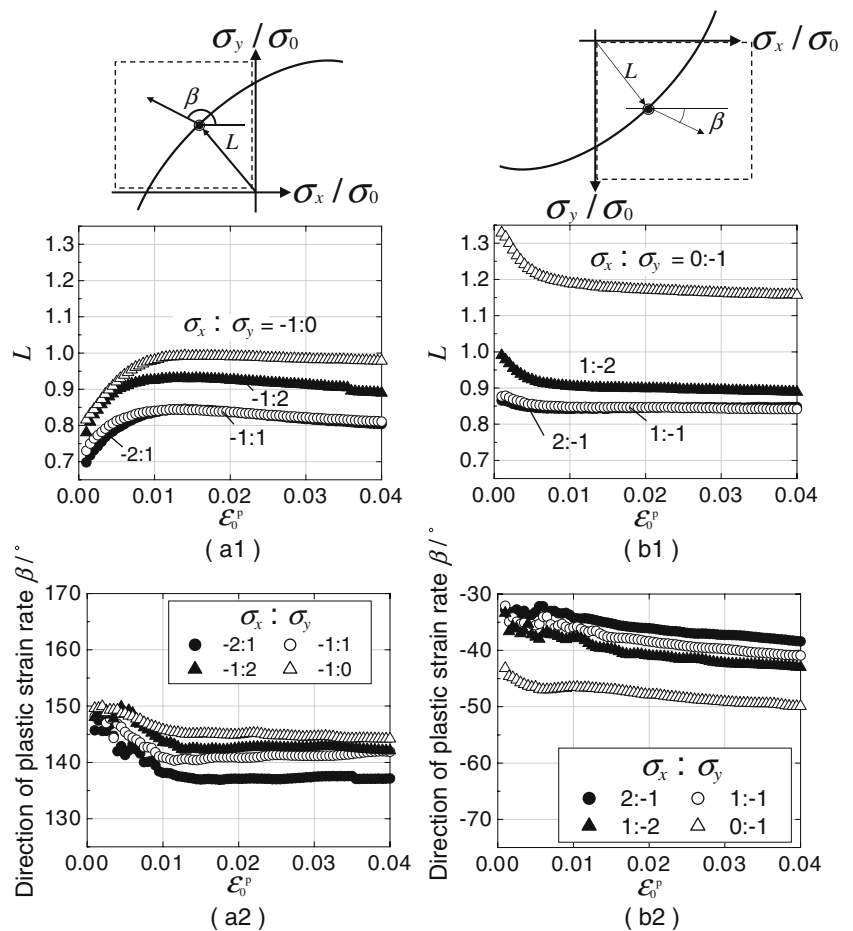
Interpolation of the relationship between the directions of plastic strain rates and loading directions

Figure 14 shows a schematic diagram of a cubic Bezier curve. A cubic Bezier curve is determined by two pass points, P_1 and P_4 , and two control points, P_2 and P_3 . The first derivatives at P_1 and P_4 are given as the slope of $\overline{P_1P_2}$ and $\overline{P_3P_4}$, respectively.

In accordance with Vegter’s method, the results of the interpolation of the stress points comprising a work contour using cubic Bezier curves is shown as a solid line in Fig. 13 (a). The interpolation curve was able to smoothly represent the work contour; however, the variation of the plastic strain rates with loading direction is not smooth at connecting points, as shown in Fig. 13 (b). Therefore, in order to ensure the smooth variation of the directions of plastic strain rates, we propose a new methodology. In the new methodology we first interpolate the directions of plastic strain rates using cubic Bezier curves. The two pass points, P_1 and P_4 , and two control points, P_2 and P_3 , in Fig. 14 are given by

$$\begin{cases} \varphi(t) = (1-t)^3\varphi_1 + 3(1-t)^2t\varphi_2 + 3(1-t)t^2\varphi_3 + t^3\varphi_4 \\ \beta(t) = (1-t)^3\beta_1 + 3(1-t)^2t\beta_2 + 3(1-t)t^2\beta_3 + t^3\beta_4 \end{cases} \quad (1)$$

Fig. 12 Variation of L and β with offset logarithmic plastic strain in the second **a** and fourth **b** quadrants of stress space, respectively. L is the length of the stress vector in stress space, from the origin to a work contour, and β is the direction of the plastic strain rate at a corresponding loading path



using a variable $t(0 \leq t \leq 1)$. Here, φ_i and β_i ($i=1$ to 4) are the direction angles of the loading direction in stress space and the plastic strain rate at point i , respectively. The Bezier curve starts at $P_1(t=0)$ and ends at $P_4(t=1)$. For simplicity, a slope α of the Bezier curve at a pass point is determined so that it coincides with that of the line connecting the adjacent pass points, as shown in Fig. 15. The length of $\overline{P_1P_2}$ and

$\overline{P_3P_4}$ were empirically determined as $2/5$ of $\overline{P_1P_4}$ in order to simplify the calculation procedure for optimization.

Description of the work contour based on the normality rule

Assuming that the material follows the associated flow rule, the directions of plastic strain rates should be parallel to the

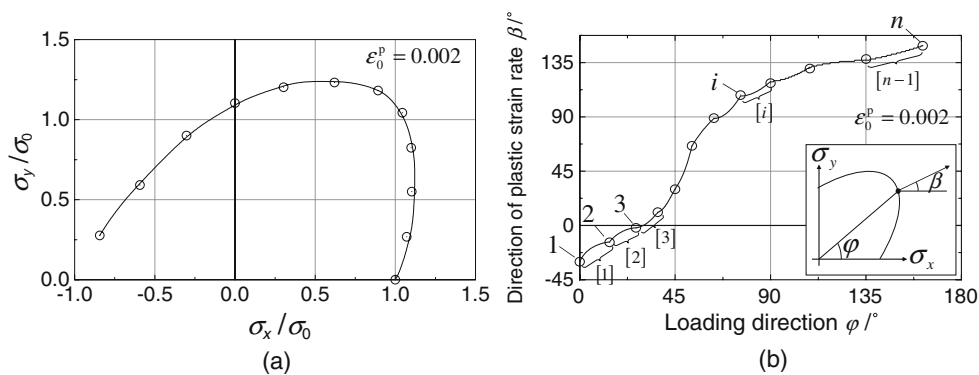


Fig. 13 A normalized work contour **a** and the directions of plastic strain rates with loading direction **b** of a steel alloy [8]. A group of cubic Bezier curve smoothly interpolates the work contour in **a**, following the calculation method proposed by Vegter and Van den

Boogaard [3]. The solid curve in **b**, which represents the directions of the outward vectors normal to the interpolation curve in **a**, lacks smoothness at the connecting points of Bezier curves in **a**

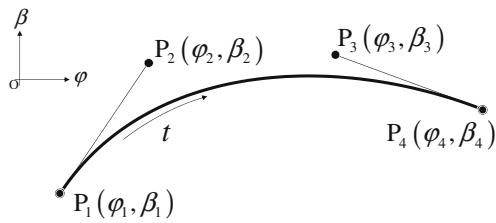


Fig. 14 A cubic Bezier curve defined using 4 points

local outward vectors normal to the work contour, provided that the work contour is assumed to coincide with a plastic potential. Then, using $\varphi(t)$ and $\beta(t)$ in Eq. 1, the work contour is given by

$$l_{[i]}(t) = l_{[i]}(0) \cdot \exp(H(t)), \quad l_{[i]}(0) \equiv l_{[i-1]}(1)$$

$$H_{[i]}(t) \equiv \int_0^t \frac{8'_{[i]}(t)}{\tan(\beta_{[i]}(t) - \delta_{[i]}(t) + \pi/2)} dt, \quad 8' \equiv d8/dt. \tag{2}$$

where l is the distance from the origin to the stress points comprising the work contour in stress space, see Appendix for the derivation of Eq. 2. $[i]$ represents the section number shown in Fig. 13 (b).

Condition of convexity of a work contour

β should increase monotonically with increasing φ , so that the convexity and smoothness of the work contour are satisfied. A tangent vector to the cubic Bezier curve $\mathbf{k}(t)$ ($0 \leq t \leq 1$) is given by a quadratic Bezier curve as

$$\mathbf{k}(t) = (1-t)^2 \overrightarrow{P_1 P_2} + 2t(1-t) \overrightarrow{P_2 P_3} + t^2 \overrightarrow{P_3 P_4}. \tag{3}$$

The condition for the monotonic increase of the tangent angle $\theta(t) (= \tan^{-1}(k_\beta/k_\varphi))$ with respect to the axis of loading direction is given as

$$0 < \theta(0), \theta(T), \theta(1) < \pi/2 \quad \because 0 < T < 1$$

$$T = \frac{\beta_1 + \beta_3 - 2\beta_2}{\beta_1 - 3\beta_2 + 3\beta_3 - \beta_4}. \tag{4}$$

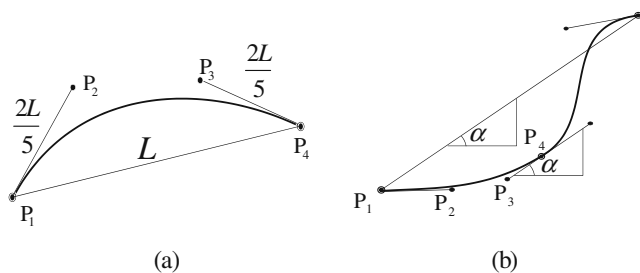


Fig. 15 Determination of the slope at a pass point on a Bezier curve

Where $\theta(0)$ and $\theta(1)$ is the tangent angles of the end points of a Bezier curve. T is t at the extremal point of $\theta(t)$ ($d\theta/dt=0$).

Error function

The Bezier curve derived from Eq. 2 does not necessarily pass through all stress points comprising the work contour shown in Fig. 13 (a). Moreover, it does not necessarily satisfy the condition of convexity. In order to correct such inconsistency, an error function is introduced as follows:

$$E = W_\beta \sum_{i=1}^n (\beta_i^{cal} - \beta_i^{exp})^2 + W_l \sum_{i=1}^{n-1} (l_i^{cal} - l_i^{exp})^2 \tag{5}$$

$$+ W_C \sum_{i=1}^{n-1} C_i C_i = c(0) + c(T) + c(1)$$

$$c(t) = \begin{cases} 0 & (0 < \theta(t) < \pi/2) \\ -\theta(t) & (\theta(t) \leq 0) \\ \theta(t) - \pi/2 & (\theta(t) \geq \pi/2) \end{cases}$$

where i is the data number shown in Fig. 13 (b), and n is the number of data. The first and second terms in Eq. 5 represent the summation of the differences between the experimental (exp) and calculated (cal) values of l_i and β_i , respectively. C_i in the third term checks the convexity of the work contour. Its value is determined from Eq. 4 and is positive when the work contour is concave. l_i^{cal} and β_i^{cal} vary during the optimization calculation in order to minimize the function E . The function is weighted by W_β , W_l and W_C . As the convexity of work contour is the first priority, W_C is greater than W_β and W_l . Additionally, $\sum C_i = 0$ should be checked after the calculation.

The approximation results based on our new methodology using cubic Bezier curves are shown as the solid lines in Fig. 16 (a) and (b). The following three cases were checked to clarify the effects of W_β and W_l on the approximation curves.

- Case 1. W_β and W_l of the error function are adjusted so that the directions of plastic strain rate can be preferentially reproduced by the approximated curves.
- Case 2. W_β and W_l are adjusted so that the general trends of the normalized work contour and the directions of plastic strain rates can be reproduced in good accuracy by the approximated curves.
- Case 3. W_β and W_l are adjusted so that the normalized work contour can be preferentially reproduced by the approximated curves.

The approximation curve for each weight condition is in good agreement with the experimental data in both graphs. There is not much difference between the three approximation

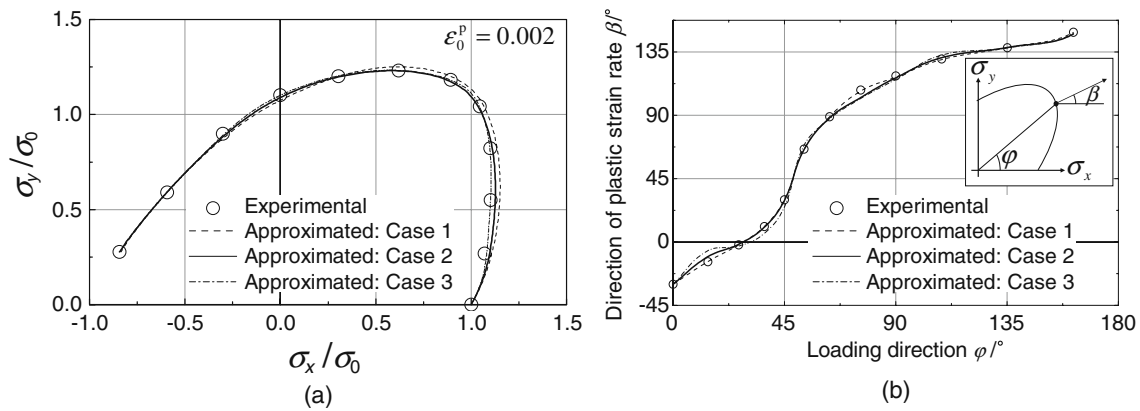


Fig. 16 Measured stress points comprising a work contour **a** and the directions of plastic strain rates **b** compared with the approximation curves calculated using the error function E as defined in “Error function”. The experimental data are quoted from [8]

results. Therefore, the approximation curve based on the new methodology can be regarded as instantaneous plastic potentials for the steel alloy, at least for linear stress paths.

Discussion

Comparison between measured data and calculated data based on selected yield functions

Figure 17 compares the measured work contours and the directions of plastic strain rates for the pure titanium sheet, measured at $\epsilon_0^p = 0.003$, with those calculated using Hill’s quadratic yield function [13], the Yld2000-2d yield function [14] and Cazacu’s yield function [15]. In order to check whether these functions are able to reproduce the large curvature of the observed work contours in the vicinity of the equibiaxial tension region, additional linear stress path tests were carried out for $\sigma_x:\sigma_y=8:7$ and $7:8$ and the measured data points were added and shown in Fig. 17. The anisotropic parameters of the yield functions used in the figure were determined using the stress values and r -values observed at $\epsilon_0^p = 0.003$. The material properties used for the determination of the anisotropic parameters of the

yield functions are shown in Table 3. r_{90} is measured to be infinite, because the thickness reduction of the test material could not be detected during the early stages of plastic deformation from the data of plastic strain increments, $d\epsilon_x^p$ and $d\epsilon_y^p$, measured using strain gauges.

The thick solid curves show the calculated results based on the Yld2000-2d yield function. As a converged solution could not be obtained using an exponent M of 6, we used $M=8$ as the exponent of the function. The calculated results are in fair agreement with the measured work contour and the directions of plastic strain rates, although the calculated results locally deviates from the measured data at the stress ratios $\sigma_x:\sigma_y=1:4\sim 1:2$ and $4:3$.

The thin solid curves show the calculated results based on Cazacu’s yield function. The exponent M of the function was taken to be 2. As Cazacu’s yield function used compressive flow stresses ($\sigma_{0-}, \sigma_{90-}$) for the determination of the anisotropic parameters, the reproducibility of the work contour in the second and fourth quadrant is superior to those for other yield functions. However, Cazacu’s yield function is not able to reproduce well the asymmetry and bulging tendency of the work contour in the first quadrant. It is noted that Cazacu and coworkers improved Cazacu’s yield function [15] and proposed a more flexible and

Fig. 17 The work contours and the directions of plastic strain rates measured at $\epsilon_0^p = 0.003$ [17], compared with those calculated using Hill’s quadratic, the Yld2000-2d and Cazacu’s yield functions

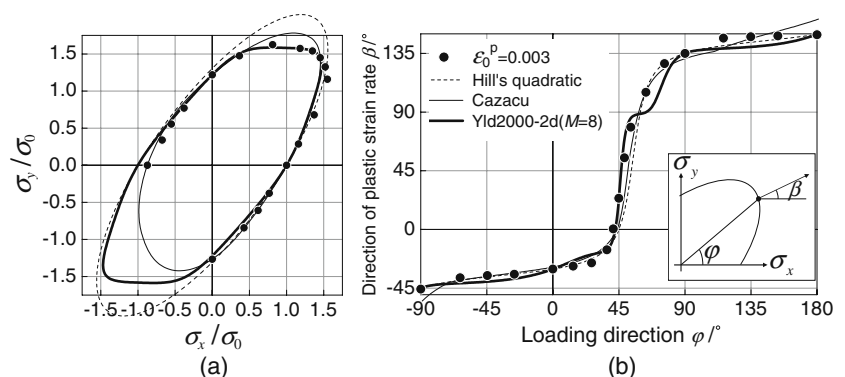


Table 3 Material properties for determining unknown parameters of anisotropic yield functions

Material property ($\varepsilon_0^p = 0.003$)		Yield function		
		Hill's quadratic	Yld2000-2d	Cazacu's
σ_0	1	○	○	○
σ_b/σ_0	1.45		○	○
σ_{90}/σ_0	1.22		○	○
$\sigma_{1:2}/\sigma_0$	0.81			○
$\sigma_{2:1}/\sigma_0$	1.37			○
σ_{0-}/σ_0	-0.87			○
σ_{90-}/σ_0	-1.27			○
r_0	1.42	○	○	
r_{90}	$+\infty$	○	○	
r_b	0.44		○	

* σ_0, σ_{90} : the uniaxial tensile stresses for the rolling direction and transverse direction, respectively
 * $\sigma_{0-}, \sigma_{90-}$: the uniaxial compressive stresses for the rolling direction and transverse direction, respectively
 * $\sigma_{1:2}, \sigma_b, \sigma_{2:1}$: the maximum principal stresses for the stress paths, $\sigma_x:\sigma_y=1:2, 1:1$ and $2:1$, respectively
 * r_0, r_{90} : the r -values for the rolling direction and transverse direction, respectively
 * r_b : the ratio of plastic strain rates, $(d\varepsilon_y^p/dt)/(d\varepsilon_x^p/dt)$, for equi-biaxial tension, $\sigma_x:\sigma_y=1:1$

accurate new yield function with a number of anisotropy coefficients using several linear transformations [16].

The dashed curves show the calculated results based on Hill's quadratic yield function. It shows large deviation from the observed work contour.

The measured work contours for $\varepsilon_0^p = 0.04$ and 0.085 were also compared with the yield loci calculated using the yield functions to verify whether these functions are able to reproduce the work hardening behavior of the test material [17]. It was found that the yield loci based on the Yld2000-

2d yield function with an exponent of 6 were in good agreement with the measured work contours .

Comparison between measured data and the approximation curve using cubic Bezier curves

The approximation method using cubic Bezier curves proposed in "Analysis method" was applied to the measured data of the pure titanium sheet [17]. Figure 18 compares the work contour and the directions of plastic strain rates in Fig. 17 with the approximation curve using cubic Bezier curves. The weights of the error functions W_β and W_l were adjusted to the three cases defined in "Error function". The approximation results based on Case 2 are generally closer to the measured data, both in Fig. 18 (a) and (b), than Cases 1 and 3 and the calculated results using anisotropic yield functions as shown in Fig. 17. However, there is still small deviation of the approximated values from the measured work contours in the vicinity of equibiaxial tension region. The cause of this discrepancy may caused by the measurement errors included in the work contour and the directions plastic strain rates.

Analysis of the differential work hardening behavior of the pure titanium using cubic bezier curves

Figure 19 (a) shows the normalized work contours of the pure titanium sheet and the corresponding optimized approximation curves for six different levels of equivalent strain ε_0^p . Figure 19 (b) shows the measured directions of plastic strain rates for each level of ε_0^p and the corresponding optimized Bezier curves. The weights of the error functions W_β and W_l were adjusted following the method of Case 2. The approximation results for each level of ε_0^p shown in Fig. 19 (a) and (b) are in good agreement with the measured data.

In order to quantitatively evaluate the reproducibility of the measured work contours by using the approximation curves,

Fig. 18 The work contours and the directions of plastic strain rates measured at $\varepsilon_0^p = 0.003$ [17], compared with the approximation curves calculated using the error function E as defined in "Error function"

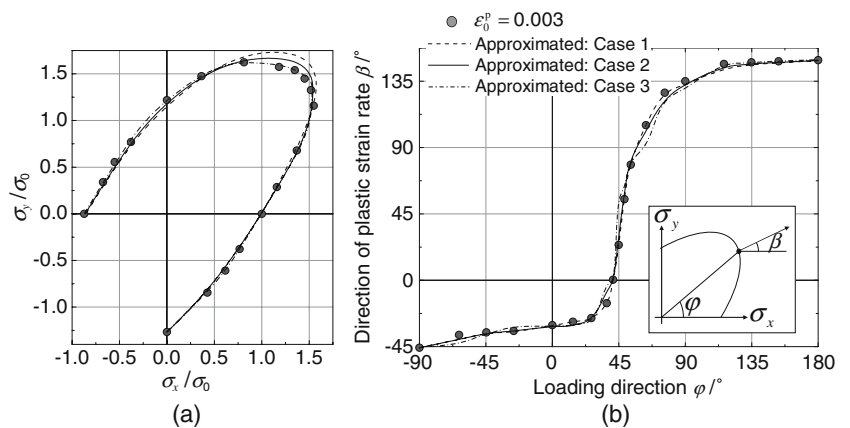
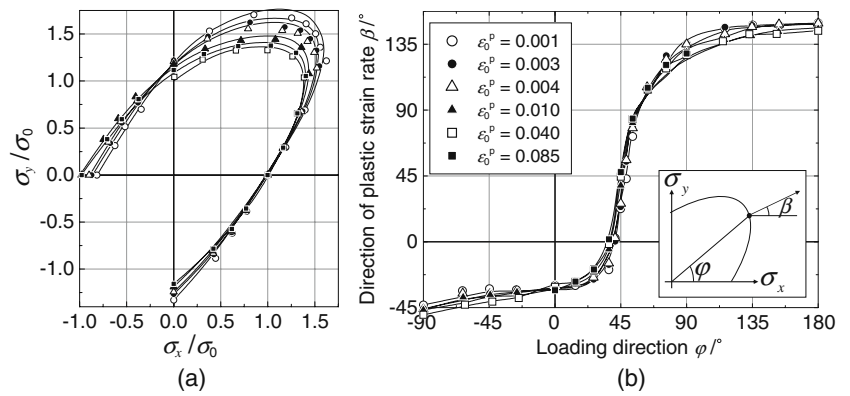


Fig. 19 The work contours and the directions of plastic strain rates measured at six different levels of ϵ_0^p [17], compared with the approximation curves calculated using the error function E as defined in “Error function”



the maximum deviation between the measured data and approximation results are shown in Fig. 20. Figure 20 (a) shows the variation of the maximum deviation of the distance L of the stress points from the origin with ϵ_0^p . For $\epsilon_0^p = 0.001$ to 0.004, the maximum deviation of L is 8~10% of the flow stress. For $\epsilon_0^p > 0.005$, the maximum deviation of L decreases with increasing ϵ_0^p and results in 4% of the flow stress. Figure 20 (b) shows the variation of the maximum deviation of the directions of measured plastic strain rates β from those of approximated with ϵ_0^p . For $\epsilon_0^p = 0.001$ to 0.004, the maximum deviation of β is nearly 10° in the range of $36^\circ \leq \varphi \leq 90^\circ$. However, the maximum deviation of β also shows drastic decrease in the vicinity of $\epsilon_0^p = 0.005$ and reduces to approximately 4.5°.

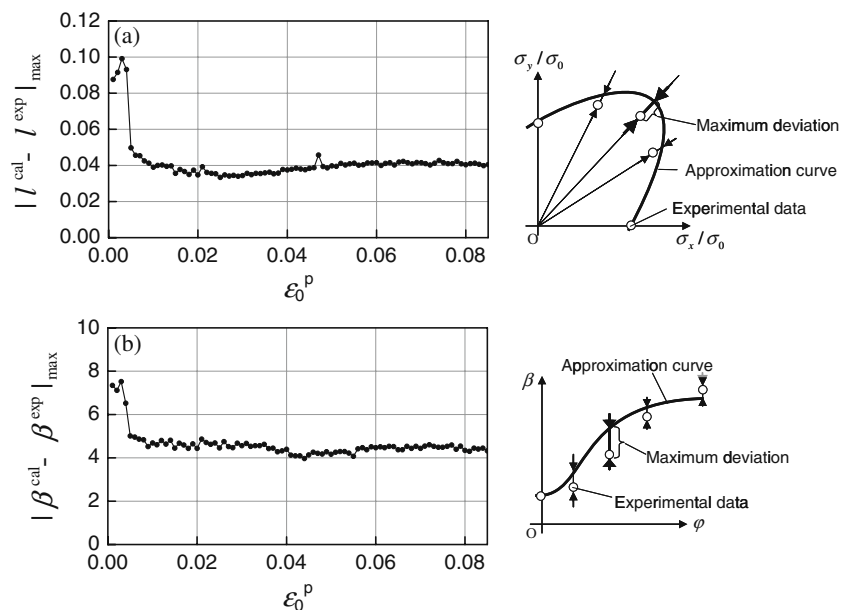
As the converged maximum deviation of L and β for $\epsilon_0^p > 0.005$ are enough small, the approximation curves in Fig. 20 (a) can be practically regarded as plastic potential at least for linear stress paths in the first, second and fourth quadrants of stress space.

Conclusion

The anisotropic plastic deformation behavior of commercial pure titanium sheet (JIS #1) was investigated for linear stress paths. The pure titanium showed significant in-plane anisotropy with respect to yield stresses and r -values. The measured plastic work contours in stress space bulged significantly in the direction of equibiaxial tension and showed significant asymmetry between the upper and lower sides of the line $\sigma_x = \sigma_y$. Moreover, the material exhibited significant differential work hardening behavior.

The measured data were compared with the calculated values using selected anisotropic yield functions, such as Hill’s quadratic yield function, the Yld2000-2d yield function and Cazacu’s yield function. We conclude that the yield functions are not able to perfectly reproduce the deformation behavior of the pure titanium under biaxial loading.

Fig. 20 Maximum deviation of the approximation curve for the work contours **a** and the directions of plastic strain rates **b** from the experimental data in Fig. 19



A method of determining the spline approximation curves that are able to reproduce both work contours and the directions of plastic strain rates was developed. The method ensures the smooth variation of the directions of plastic strain rates with stress ratios. The method was successfully applied to the analysis of the work hardening behavior of the pure titanium sheet. The calculated results using the approximation curves were closer to the measured work contour and the directions of plastic strain rates of the pure titanium than those calculated using the selected anisotropic yield functions. Consequently, we conclude that the approximation curves for the measured work contours can be practically regarded as plastic potentials at least for linear stress paths.

By applying the approximation curves to the measured data of work contours and the directions of plastic strain rates for different levels of ε_0^p , the details of the differential work hardening behavior of the pure titanium was successfully revealed. The analyzed data will be useful for the formulation of the differential work hardening behavior of the pure titanium.

Acknowledgements We express deep appreciation to the Nonferrous Metals Division of the Ministry of Economy, Trade and Industry for the assistance rendered in various aspects of this research.

Appendix: derivation of Eq. 2

When the coordinates of stress points making up a work contour in stress space are given in polar coordinates ($\sigma_x = l \cos \varphi$, $\sigma_y = l \sin \varphi$), a slope of a tangent to the work contour is given by

$$\frac{d\sigma_y}{d\sigma_x} = \frac{l' \sin \varphi + l \cos \varphi}{l' \cos \varphi + l \sin \varphi}, \quad (\text{A.1})$$

where l is expressed as a function of φ . $l' \equiv dl/d\varphi$.

From the associated flow rule, a slope of a tangent to the work contour is determined as

$$\frac{d\sigma_y}{d\sigma_x} = \tan\left(\beta + \frac{\pi}{2}\right), \quad (\text{A.2})$$

using the direction of plastic strain rate β . From Eqs. A.1 and A.2,

$$\begin{aligned} \frac{l'}{l} &= \frac{\tan(\beta + \pi/2) \sin \varphi + \cos \varphi}{\tan(\beta + \pi/2) \cos \varphi - \sin \varphi} \\ &= \frac{1}{\tan(\beta - \varphi + \pi/2)}. \end{aligned} \quad (\text{A.3})$$

Indefinite integral of Eq. A.3 with respect to φ leads to

$$\ln l + C = \int \frac{1}{\tan(\beta - \varphi + \pi/2)} d\varphi \quad (\text{A.4})$$

Expressing β and φ using the cubic Bezier curve parameter, t , l is given as

$$\ln l + C = \int \frac{\varphi'}{\tan(\beta - \varphi + \pi/2)} dt \quad (\text{A.5})$$

$$l(t) = l_0 \exp\left(\int_0^t \frac{\varphi'}{\tan(\beta - \varphi + \pi/2)} dt\right),$$

where $\varphi' \equiv d\varphi/dt$.

References

1. Kuwabara T (2007) Advances in experiments on metal sheets and tubes in support of constitutive modeling and forming simulations. *Int J Plast* 23:385–419
2. Hill R, Hecker SS, Stout MG (1994) An investigation of plastic flow and differential work hardening in orthotropic brass tubes under fluid pressure and axial load. *Int J Solid Struct* 31(21):2999–3021
3. Vegter H, Van den Boogaard AH (2006) A plane stress yield function for anisotropic sheet material by interpolation of biaxial stress states. *Int J Plast* 22:557–580
4. Kuwabara T, Katami C, Kikuchi M, Shindo T, Ohwue T (2001) Cup drawing of pure titanium sheet-finite element analysis and experimental Validation-. *Proc 7th Int Conf Numerical Methods in Industrial Forming Processes*: pp 781–787.
5. Kuwabara T, Ikeda S, Kuroda K (1998) Measurement and analysis of differential work hardening in cold-rolled steel sheet under biaxial tension. *J Mater Process Tech* 80–81:517–523
6. Kuwabara T, Ishiki M, Kuroda M, Takahashi S (2003) Yield locus and work-hardening behavior of a thin-walled steel tube subjected to combined tension-internal pressure. *J Phys IV* 105:347–354
7. Kuwabara T, Yoshida K, Narihara K, Takahashi S (2005) Anisotropic plastic deformation of extruded aluminum alloy tube under axial forces and internal pressure. *Int J Plast* 21–1:101–117
8. Kuwabara T, Horiuchi Y, Uema N, Ziegelheimova J (2008) Material testing method of applying in-plane combined tension-compression stresses to sheet specimen. *IDDRG '08*: pp 163–171
9. Lee D, Backofen WA (1966) An experimental determination of the yield locus for titanium and titanium-alloy sheet. *Trans AIME* 236:1077–1054
10. Kuwabara T, Morita Y, Miyashita Y, Takahashi S (1995) Elastic-plastic behavior of sheet metal subjected to in-plane reverse loading. *Proc fifth international symposium on plasticity and its current applications*: pp 841–844
11. Kuwabara T, Kumano Y, Ziegelheim J, Kurosaki I (2009) Tension-compression asymmetry of phosphor bronze for electronic parts and its effect on bending behavior. *Int J Plast* 25:1759–1776
12. Kuwabara T, Van Bael A, Iizuka E (2002) Measurement and analysis of yield locus and work hardening characteristics of steel sheets with different r-values. *Acta Mater* 50(14):3717–3729
13. Hill R (1948) A theory of the yielding and plastic flow of anisotropic metals. *Proc Roy Soc London A* 193:281–297
14. Barlat F, Brem JC, Yoon JW, Chung K, Dick RE, Lege DJ, Pourboghraat F, Choi S-H, Chu E (2003) Plane stress yield function for aluminum alloy sheet—part1: theory. *Int J Plast* 19(9):1297–1319
15. Cazacu O, Plukett B, Barlat F (2006) Orthotropic yield function for hexagonal closed packed metals. *Int J Plast* 22:1171–1194
16. Plunkett B, Cazacu O, Barlat F (2008) Orthotropic yield criteria for description of the anisotropy in tension and compression of sheet metals. *Int J Plast* 24:847–866
17. Ishiki M, Kuwabara T, Yamaguchi M, Maeda Y, Hayashida Y (2008) Differential work hardening Behavior of pure titanium sheet under biaxial loading. *7th International conference and workshop on Numerical Simulation of 3D Sheet Metal Forming Processes*: pp 161–166